Available online at www.sciencedirect.com
SCIENCE DIRECT®
Journal of Electron Spectroscopy and Related Phenomena 137–140 (2004) 785–794
JOURNAL OF ELECTRON SPECTROSCOPY and Related Phenomena
www.elsevier.com/locate/elspec

# Selective adsorption of protein on polymer surfaces studied by soft X-ray photoemission electron microscopy

C. Morin [a], A.P. Hitchcock [a,*], R.M. Cornelius [a], J.L. Brash [a], S.G. Urquhart [b], A. Scholl [c], A. Doran [c]

[a] *Department of Chemistry, BIMR, McMaster University, 1280 Main Street West, Hamilton, Ont., Canada L8S 4M1*
[b] *Department of Chemistry, University of Saskatchewan, Sask., Canada S7N 5C9*
[c] *Advanced Light Source, Berkeley Lab, Berkeley, CA 94720, USA*

Available online 28 March 2004

**Abstract**

X-ray photoemission electron microscopy (X-PEEM) using synchrotron radiation illumination in the C 1s, N 1s and O 1s regions has been used to characterize a phase segregated polystyrene/polymethylmethacrylate (PS/PMMA) polymer thin film, and to map the adsorption of fibrinogen (a blood plasma protein) on this surface from both isotonic, buffered, and low ionic strength, unbuffered aqueous solutions at varying fibrinogen concentrations. The concentration dependence of the coverage correlates with independent, non-spatially resolved measurements using $^{125}$I-radiolabeled protein. At low concentrations (<0.1 mg/ml) of the buffered solution, adsorption of fibrinogen occurs with strong preference for PS domains. In contrast, adsorption from similar concentrations of unbuffered solution strongly prefers the interface of the PS and PMMA domains. Increasing the solution concentration up to 1 mg/ml of both buffered and unbuffered solutions leads progressively to full surface coverage (close-packed monolayer). These results demonstrate for the first time that X-PEEM with tunable soft X-rays has the sensitivity to locate and detect adsorbed proteins at the submonolayer level, while simultaneously detecting the spatial distribution of phases, and protein distribution relative to the phases, at the surface of an underlying microphase separated polymer substrate.


*Keywords:* Photoemission electron microscopy; Protein mapping; Polystyrene; Polymethylmethacrylate blend; Polymer thin films; Biomaterials

## 1. Introduction

The biocompatibility of a material is believed to be related to the properties of the first protein layer adsorbed on contact with biological tissue or fluids. Initially adsorbed proteins mediate the subsequent interactions of cells with the surface [1]. It is envisioned that novel surfaces that direct the biological healing process would have a well-defined array of biorecognition sites designed to interact specifically with cells since many of the important functions of cells depend on the type and orientation of molecules at their surfaces. In other cases, such as artificial materials used for blood contact, unfavorable aspects of first-layer protein adsorption can lead to coagulation, complement activation and other adverse responses [2]. Thus, techniques which can map submonolayer amounts of adsorbed proteins at high spatial resolution, and thereby identify preferred sites of protein attachment on heterogeneous substrates, are of interest to assist understanding of biocompatibility issues and the development of improved biomaterials.

We are exploring the strengths and limitations of a number of soft X-ray microscopies for this purpose. Earlier we have shown that scanning transmission X-ray microscopy (STXM) can detect protein at near monolayer coverage adsorbed on structured polymers, even in the presence of a few micron overlayer of aqueous buffer [3]. While the ability to study wet systems is very attractive for approximating real world biomaterial–biological interfaces, the sensitivity to the actual polymer–protein interface is limited since the interface is only one part of the signal measured in a transmission experiment. The sampling depth of X-ray photoemission electron microscopy (X-PEEM) is ~10 nm, and thus X-PEEM, while a vacuum technique like XPS, should have significantly higher surface sensitivity than STXM and perhaps be better suited for this purpose. Here, we report first explorations of X-PEEM for studies of protein adsorption. The test substrate is a phase segregated blend of polystyrene (PS) and polymethylmethacrylate (PMMA), spun cast as a

* Corresponding author. Tel.: +1-905-525-9140x24749; fax: +1-905-521-2773.
*E-mail address:* aph@mcmaster.ca (A.P. Hitchcock).

0368-2048/$ – see front matter © 2004 Elsevier B.V. All rights reserved.
doi:10.1016/j.elspec.2004.02.158

thin film on a Si wafer. We recently reported a detailed characterization of spun cast thin film PS/PMMA blends by atomic force microscopy (AFM), PEEM and STXM [4]. The test protein for investigating selective adsorption on this surface is fibrinogen (Fg), a 340 kDa plasma protein that plays a central role in coagulation and thrombosis [5]. Fibrinogen adsorption from blood plasma is unusual in that more fibrinogen is adsorbed on most materials in a short exposure (10 s) than lengthy (1 h) contact times [6]. Also, more fibrinogen adsorbs from intermediate plasma dilutions than from either highly diluted or undiluted plasma. These phenomena, collectively called the "Vroman effect" [5], are intriguing and suggest that fibrinogen molecules, once adsorbed, are eventually displaced from the surface by other adsorbing plasma proteins. While that concentration and exposure time-dependent behavior is specific for fibrinogen adsorption from the complex mixture of proteins present in plasma, it is interesting to measure adsorption from pure fibrinogen solutions as a reference point for the more complex, mixed protein plasma system, which will eventually be the target for study.

Measurements were performed using the electrostatic PEEM at the Advanced Light Source (ALS, Berkeley, CA) [7], and a magnetic PEEM at the Synchrotron Radiation Center (SRC, University of Wisconsin at Madison). Here, we describe only the ALS results due to space limitations. We have recorded images, spectra, and image sequences in the C 1s, N 1s and O 1s regions on annealed PS/PMMA thin films both before and after exposure to fibrinogen. The protein adsorption was carried out from a phosphate buffer (pH 7.2) at concentrations from 0.005 to 1 mg/ml, and from low ionic strength, unbuffered aqueous solutions at 0.05 and 0.1 mg/ml (pH 6.6–6.9 with protein present). Adsorption isotherm studies by $^{125}$I-radiolabeling and atomic force microscopy studies were also carried out. Detailed analysis of the PEEM results shows that, in the low concentration limit, fibrinogen prefers the continuous PS domains when adsorbed from a buffer solution, but shows a distinct preference for the PS/PMMA interface when adsorbed from non-buffered solution.

## 2. Experimental

### 2.1. Materials and methods

#### 2.1.1. Substrate

PS (MW $= 1.07 \times 10^6$ dalton, $\delta = 1.06$) and PMMA (MW $= 0.31 \times 10^6$ dalton, $\delta = 1.01$) were obtained from Polymer Source Inc. and were used without further purification. A 28:72 (w/w) PS/PMMA (1% by weight) toluene (Aldrich, 99.8% anhydrous) solution was spun cast (∼50 μl drop, 4000 rpm, 30 s) onto clean 1 cm × 1 cm native oxide Si (1 1 1) wafers (Wafer World Inc.), which had previously been degreased with trichloroethylene (Aldrich, >99.5% pure), acetone (Burdick & Jackson, HPLC grade), and methanol (Caledon), then rinsed under running Milli-Q water. The PS:PMMA/Si substrates were annealed at 160 °C for 8 h in a vacuum oven with pressure $\sim 10^{-2}$ Torr. Non-contact mode AFM measurements of the PS:PMMA substrate and several Fg/PS:PMMA samples were made in the region of the $I_0$ normalization scratch. These showed the polymer film is 40–50 nm thick with 5–10 nm (rms) corrugation in the PS:PMMA pattern. The adsorbed fibrinogen could not be reliably detected by our AFM measurements, probably because of the softness of the polymer substrate, combined with a corrugation that is similar in size scale to the size of the adsorbed proteins.

#### 2.1.2. Protein

Plasminogen-free human plasma fibrinogen (Calbiochem) was used; dialysis to remove possible low-molecular-weight impurities was performed for the radiolabeling but not the PEEM samples. It is reported to be >95% clottable by thrombin, and pure as judged by SDS-PAGE. Solutions for exposure to PS:PMMA were made at various concentrations in two different solvents, deionized water and phosphate buffer (Pierce, No. 28372, 0.1 M sodium phosphate and 0.15 M sodium chloride; when a pouch is dissolved in 500 ml deionized water, the pH is 7.2).

### 2.2. Methods

#### 2.2.1. X-PEEM

X-PEEM of organic materials is challenging on account of potential problems with charging, field emission, and radiation damage. We have worked extensively to optimize our sample preparation, data acquisition, and data analysis procedures [8] to the point where we can measure many systems with minimal artifacts. Aspects important in this work are: keeping the PS:PMMA layer thin (<50 nm) and flat (∼10 nm rms); using an internal reference (scratch through the film to expose Si for $I_0$ determination); use of a Ti filter to reduce second order radiation in C 1s region; use of beamline masks to decrease flux on the sample (at ALS beamline 7.3.1, the peak flux is $\sim 10^{10}$ photons/s at 400 eV in a 30 μm × 30 μm spot). We have characterized the radiation damage rates for all three components [9]. As expected, PMMA is the most sensitive. Under the conditions used (masking to <∼5% of full flux), a 120 s measurement time leads to about 1/10th of saturation damage. In order to have sufficient spectral definition and statistical precision, most of these measurements were made with a total exposure time ranging between 120 and 180 s, of which less than 50% of the time is used to acquire ∼60 images, each with 1 s exposure, the remainder being overhead associated with data transfer and monochromator movement. With the masking conditions used the bending magnet beam is elliptically polarized with 70–80% right circularly polarized light. The electrostatic field at the sample was typically 9 kV/mm, but this sometimes had to be reduced to as low as 8 kV/mm, in cases of mild charging. The intermediate voltage was then

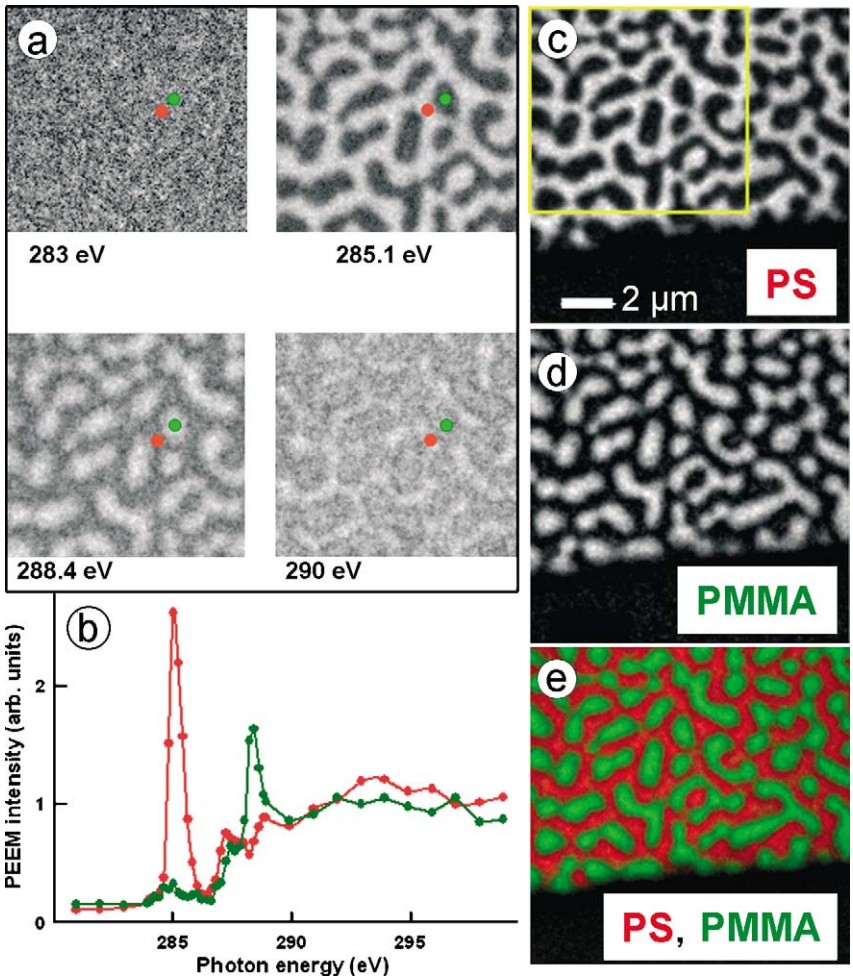


Fig. 1. (a) X-PEEM images at 283, 285.1, 288.4 and 290 eV, 4 of the 40 images in the C 1s region of an annealed 28:72 (w/w) PS:PMMA blend thin film spun cast on native oxide Si (note the actual average surface composition is 57:43; see text). (b) Spectra from the indicated spots. (c and d) Component maps of PS and PMMA derived by singular value decomposition of the C 1s image sequence. (e) Color coded composite map (red: PS; green: PMMA).

adjusted such that the resulting field-of-view was between 40 and 60 μm. The energy scales were calibrated from the known positions of the PS, PMMA and Fg structures [8,13]. The incident flux signal was taken from the region of a scratch through the polymer film (see Fig. 1) for the C 1s and N 1s edges, and from the signal from a downstream Au mesh for the O 1s edge. The $I_0$ signals were corrected for the elemental photoabsorption response of Si or Au [10].

Image sequences (stacks) were prepared for analysis by: (1) energy calibration; (2) normalization to the elemental-corrected $I_0$; and (3) scaling the intensity to match to the elemental photoabsorption response of the substrate polymer, $C_5H_8O_{1.4}$ [10], based on the nominal 30:70 PS:PMMA stoichiometry. Assuming the work function is not strongly affected by the differing amounts of adsorbed protein, this approach should give an approximately quantitative analysis (percent composition of the region sampled) since the model spectra used in the analysis are placed on a linear absorption scale (signal per nm) which is set by matching to the elemental response. Component maps for PS, PMMA and Fg were then derived from these calibrated, normalized image sequences by either singular value decomposition (SVD) [11] or stack fit [12] fitting routines, within the aXis2000 X-ray microscopy analysis package [13]. Stack fit gave statistically better fits than SVD since it incorporates an additional constant term which accommodates uncorrected backgrounds such as those from camera offsets, and possibly some long escape depth signal from the underlying Si wafer. For the C 1s and O 1s edges, fits were made to three components (PS, PMMA and Fg) while for the N 1s edge, the fit was made only to two components (PS and Fg) since the PS and PMMA are indistinguishable in this energy region.

### 2.2.2. *Protein exposure*

For X-PEEM, the Fg/PS:PMMA samples were prepared by 10 min incubation of the PS:PMMA substrate in ∼2 ml of Fg solution contained in a Fisher multi-well plate (1 cm diameter wells), followed by continuous dilution of the overlayer solution with running deionized water for ∼3–5 min. The Fg/PS:PMMA substrate was then removed from the

well. This rinsing method was used to avoid depositing protein or buffer salts from the air–solution interface.

#### 2.2.3. Experiments with radiolabeled fibrinogen

Fibrinogen was labeled with $^{125}$I (ICN Biomedicals, Mississauga, Ont., Canada) using the iodogen technique [14], a standard protocol for radioiodination of proteins by IODO-GEN® (Pierce Chemical Company, Rockford, IL) [15]. The labeled protein was dialyzed overnight against isotonic Tris buffer to remove unbound radioactive iodide. Trichloroacetic acid precipitation [16] of aliquots of protein solutions before and after completion of the experiments confirmed that >99% of the $^{125}$I remained bound to the protein. The adsorption experiments were carried out in phosphate buffered saline (pH 7.2) with four repeats and in Milli-Q water (three repeats), also for 10 min exposures. For the radiolabeling experiments, the samples were rinsed statically for 2.5 min in a similar volume of buffer solution, and three times more for 2.5 min each in Milli-Q water. Adsorbed amounts were calculated as described earlier [17]. For the blend surface, it was demonstrated that batch rinsing and continuous rinsing gave the same adsorption isotherm.

## 3. Results

### 3.1. PS:PMMA substrate

Fig. 1 presents selected energy images and selected region C 1s spectra measured with X-PEEM. The raw images show the PS:PMMA phase segregated pattern only at the energies of strong PS (285.1 eV) and strong PMMA (288.5 eV) absorption peaks, with contrast inversion. Fig. 1 also presents PS and PMMA component maps derived from singular value decomposition analysis [11] of the C 1s image sequence and a color composite map. X-ray damage to PMMA [9] results in loss of C=O bonds, leading to intensity loss at 288.5 eV, and formation of C=C bonds, leading to intensity gain at 285 eV. The C 1s image sequence for PS:PMMA was measured for 140 s, about the time for ∼10% of saturation damage, and thus should have a barely detectable signal at 285 eV. In fact the PMMA domains do exhibit a significant 285.1 eV signal. In this particular example very little of the 285 eV signal is from radiation damage; the majority is associated with PS micro-domains embedded in the PMMA macro-domains [4] which, to date, are an unavoidable feature of our sample preparation. Based on analysis of the C 1s spectrum averaged over large areas, the composition in the depth sampled by X-PEEM (estimated as 5–10 nm) is 57(2):43(2) (w/w), significantly enriched in PS relative to the formulation, as found earlier [4].

Table 1 reports the advancing water contact angles for the pure PS, pure PMMA and the PS:PMMA blend surface. Pure PS is more hydrophobic than pure PMMA. The water contact angle for PS:PMMA falls at an intermediate value, one that is consistent with the actual 57:43 surface composition, as opposed to the 28:72 formulation.

Table 1
Advancing water contact angle[a] for PS, PMMA and PS:PMMA

| Sample | Angle on sample[b] | Literature |
|---|---|---|
| PS | 77.5(4) | 86 [23] |
| PS:PMMA | 74.9(8) | – |
| PMMA | 70.7(3) | 62–73 [24] |

[a] Advancing water contact angles were measured using the sessile drop method. Milli-Q water and a Ramé-Hart (Mountain Lakes, NJ) NRL goniometer were used for these measurements.
[b] Error in last digit is based on spread of two measurements.

### 3.2. $^{125}$I-Fg on PS:PMMA adsorption isotherms

Fig. 2 shows isotherms for adsorption of $^{125}$I-labeled Fg from phosphate buffer to pure PS, to pure PMMA and to the PS:PMMA blend surface. Across the entire concentration range there is a significantly greater amount of Fg adsorbed to the PS than to the PMMA, while the blend surface adsorbs an intermediate amount. The adsorbed amounts at the higher concentrations are in the range of close-packed monolayers. The higher amounts on PS occur not just at monolayer saturation but also in the low concentration regime. This suggests that, for the 10 min exposure time used, the adsorbed amount on the three different surfaces reflects relative binding affinities rather than any kinetic effect. The adsorption behavior as monitored by $^{125}$I-labeling, is also sensitive to the ionic strength of the adsorbing solution. As shown in the inset to Fig. 2, the slope of the isotherm in the <0.1 mg/ml regime for Fg adsorption from buffer is ∼1.5× as steep as that for Fg adsorption from water. For adsorption from buffer these

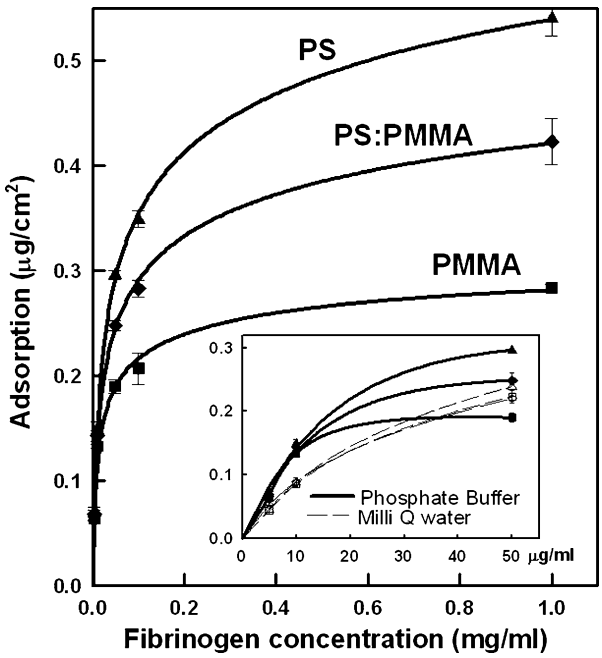


Fig. 2. Isotherms for adsorption of $^{125}$I-labeled Fg from phosphate buffer (pH 7.2) to pure PS, pure PMMA and the PS:PMMA blend surface. The inset compares the isotherms at low concentration from phosphate buffer and water.

results suggest that for the PS:PMMA blend, Fg will adsorb preferentially to PS rather than to PMMA domains. However, the data also indicate there is no preference when the solvent is water, at least for concentrations up to 50 μg/ml.

### 3.3. X-PEEM of Fg/PS:PMMA

#### 3.3.1. Reference spectra

Fig. 3 shows the NEXAFS spectra of pure PS, PMMA and Fg spun cast thin films in the C 1s, N 1s and O 1s regions, recorded with X-PEEM. The intensity scales in each panel (core edge) are on the same scale (aside from the offsets introduced for clarity) but the scales are set independently from panel to panel to allow proper viewing of the spectra. The dotted lines are the expected elemental responses [10]. All three materials exhibit distinct C 1s spectra. The Fg and PMMA spectra are each dominated by C 1s (C=O) $\rightarrow \pi^*_{C=O}$ transitions. However, the $\pi^*_{C=O}$ peak in Fg occurs 0.3 eV below the $\pi^*_{C=O}$ peak in PMMA since the carbonyl carbon is in a less electronegative environment (CONH versus COOR). Due to the small size of this shift and the otherwise similar nature of the Fg and PMMA C 1s spectra, accurate energy calibration is essential for reliable analysis. Addition of signal from the N 1s and O 1s edges significantly enhances the ability of NEXAFS to differentiate these species. Only Fg has a N 1s spectrum, with a characteristic N 1s $\rightarrow \pi^*_{CONH}$ transition at 401.2 eV, as found in other proteins and peptides [18,19]. At the O 1s edge, PMMA and Fg each are dominated by O 1s $\rightarrow \pi^*_{C=O}$ transitions at 531.6 eV, but PMMA has an extra transition at 535.5 eV arising from O 1s (O–$CH_3$) $\rightarrow \pi^*_{C=O}$ transitions, specific to esters.

#### 3.3.2. Fg(buffer)/PS:PMMA

Fig. 4 presents results of a stack fit analysis of the C 1s image sequence for Fg adsorption from 0.05 mg/ml buffer solution. In the composite map (a), pure red indicates 100% PS, pure green indicates 100% PMMA and pure blue indicates 100% Fg in the region sampled. Due to the finite sampling depth both adsorbed protein and underlying polymer substrate may contribute. If so, this would be indicated by intermediate colors (purple for Fg and PS or turquoise for Fg and PMMA). Fig. 4a shows the continuous PS domains to be purple rather than red, whereas the PMMA domains are pure green with a few isolated blue dots on the PMMA. This indicates that there is a much larger amount of Fg present on the PS domains than on the PMMA domains. The pattern of the main signal in the Fg component map (Fig. 4d) matches that of the continuous PS domains, not the discrete PMMA domains, also indicating that Fg sits preferentially on the PS domains. Note that the smallest regions with detectable protein signal are about 200 nm, ~4 times the size of a single protein [20], indicating that with improved signal quality and spatial resolution it may be possible to map single protein molecules with X-PEEM. Fig. 4e, 4f and 4g are spectra of the pixels in the regions indicated by the color outlines in the grayscale component maps (Fig. 4b–d), which were selected using threshold masking of the component maps. Fig. 4e–g also show the results of curve fits of these selected-area spectra to the reference spectra plotted in Fig. 3. This analysis indicates detectable Fg signal in the high-PS pixels, and strong PS-signal in the high-Fg pixels, but very little Fg in the high-PMMA pixels. Thus, the preference for Fg to adsorb on the PS rather than the PMMA domains is fully supported by the spectral analysis.

The numerical results for fits to the spectra of the PS-rich, PMMA-rich and Fg-rich regions for all four Fg(buffer)/PS:PMMA systems studied are presented in Table 2. For the 0.05 mg/ml Fg(buffer) system quantitative spectral analysis indicates that the center of the PS domains contain ~20% Fg. Similarly, the spectrum of pixels with strong Fg components is analyzed to contain 45% PS and negligible amounts of PMMA. Finally, the center of the PMMA domains is dominated by PMMA (70%) with the remaining signal mostly PS (21%), probably associated

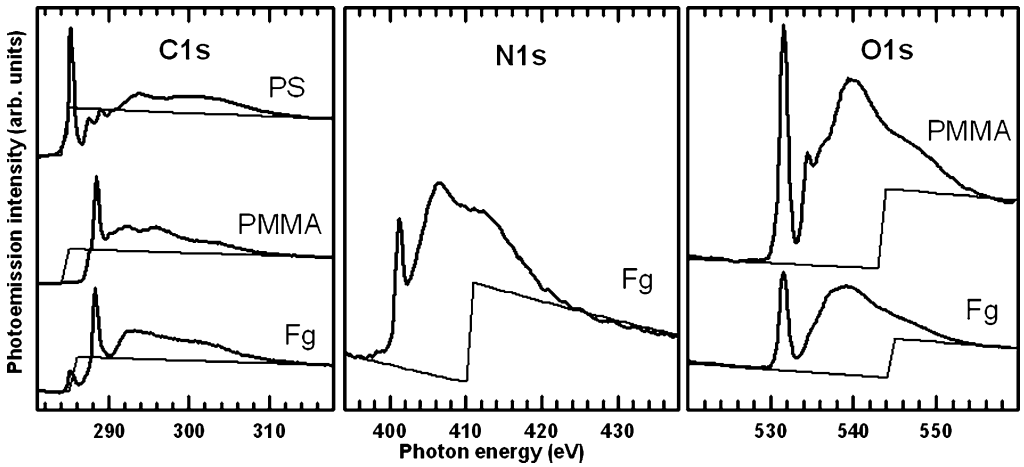


Fig. 3. C 1s, N 1s and O 1s NEXAFS spectra of PS, PMMA and Fg recorded as pure materials with X-PEEM. The dashed lines indicate the elemental response [10]. The intensities within each panel are on the same scale, although offsets are used for clarity. Different scaling is used for each panel.

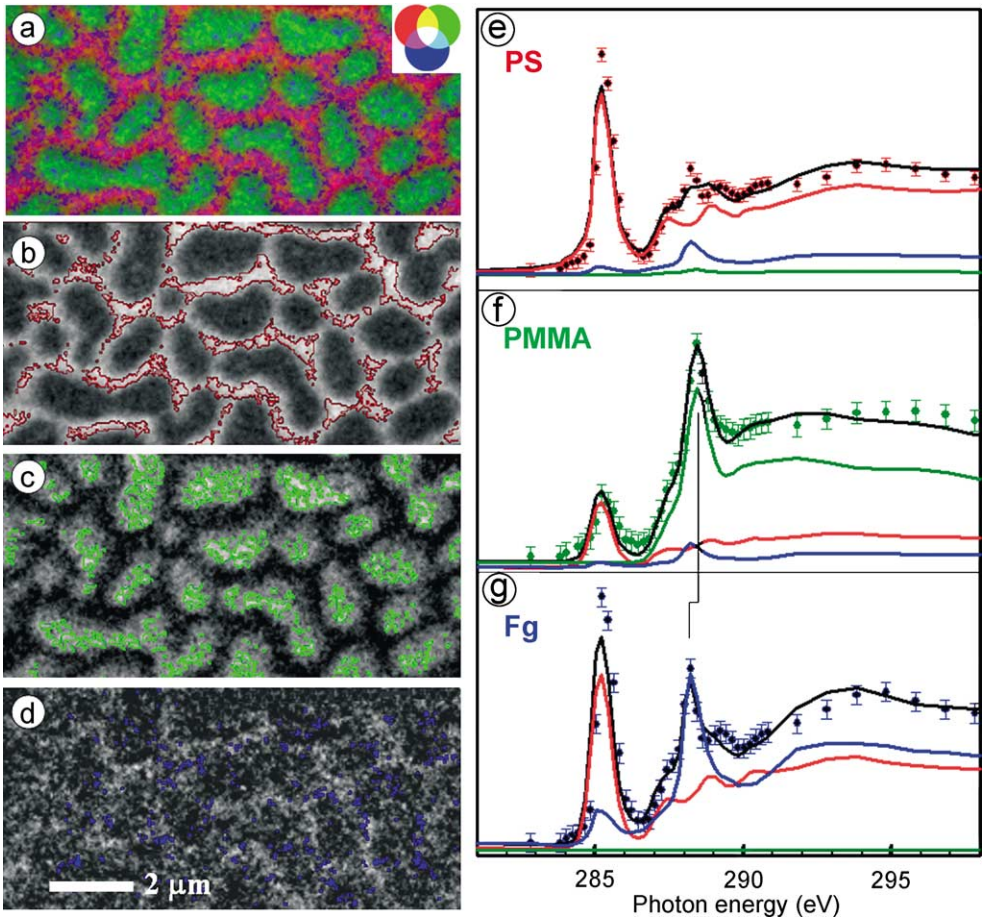


Fig. 4. (a) Composite map (red: PS; green: PMMA; blue: Fg) derived from component maps extracted by stack fit analysis of a C 1s image sequence for fibrinogen (0.05 mg/ml in buffer) adsorbed on the PS:PMMA blend surface. (b–d) Component maps indicating the regions from which spectra of high-PS, high-PMMA and high-Fg signals were extracted and displayed in (e–g) which also plot the curve fits of the extracted spectra (dots: data; black line: sum of component signals; colored lines: component signals). Most of the 285 eV signal in the spectrum of the PMMA-rich pixels comes from radiation damage.

with micro-domain PS [4], although possibly also reflecting some radiation damage. One should be careful to differentiate between "first site of adsorption", "sparse occurrence of Fg on PMMA" and "where most of the protein sits". The latter is what our analysis is indicating. It is possible there is a preference for the PS/PMMA interface as the first site of adsorption (see further). However, we base our interpretation "Fg prefers PS when adsorbed from buffered solutions" on the dominant site of Fg attachment in the stable, equilibrium system. N 1s and O 1s image sequences were also measured for some of the systems (results not shown) and these results are consistent with a preference for Fg adsorption on PS rather than PMMA at low concentrations.

Fig. 5 shows the C 1s spectra extracted for pixels of high PS (a) and high Fg (b), for four concentrations between 0.005 and 1.0 mg/ml of Fg(buffer). For the lowest protein concentration, the high-PS region spectrum is very similar to that of pure PS, while for the same concentration, the high-Fg has a strong PS signature, consistent with its location on the PS domains, as shown by the mapping in Fig. 4. As the protein concentration increases to 1.0 mg/ml, the high-PS spectra show an increasing 288.2 eV $\pi^*_{C=O}$ peak from the Fg. For adsorption from a 1.0 mg/ml solution, the Fg signal is stronger than that for PS. As expected, the C 1s spectrum of high-Fg pixels becomes progressively more like pure Fg as the Fg concentration increases. Also, the high-Fg pixels are spread over increasingly large areas as the concentration increases, and the high-Fg location changes from "dominantly on PS" for the two lowest concentrations, to nearly full surface coverage at 1.0 mg/ml. The corresponding results for the PMMA-rich pixels are consistent with the conclusion of PS-preference at low coverage, and whole-surface coverage at high concentration. However, the plots are not shown since the high-PMMA spectra for exposure from low concentration Fg(buffer) solutions are significantly distorted by radiation damage.

### *3.3.3. Fg(water)/PS:PMMA*

Fig. 6 presents color composite maps derived by stack fit analysis of C 1s, N 1s and O 1s image sequences recorded for Fg adsorption from 0.05 mg/ml unbuffered, low ionic strength aqueous solution. In contrast to the corresponding

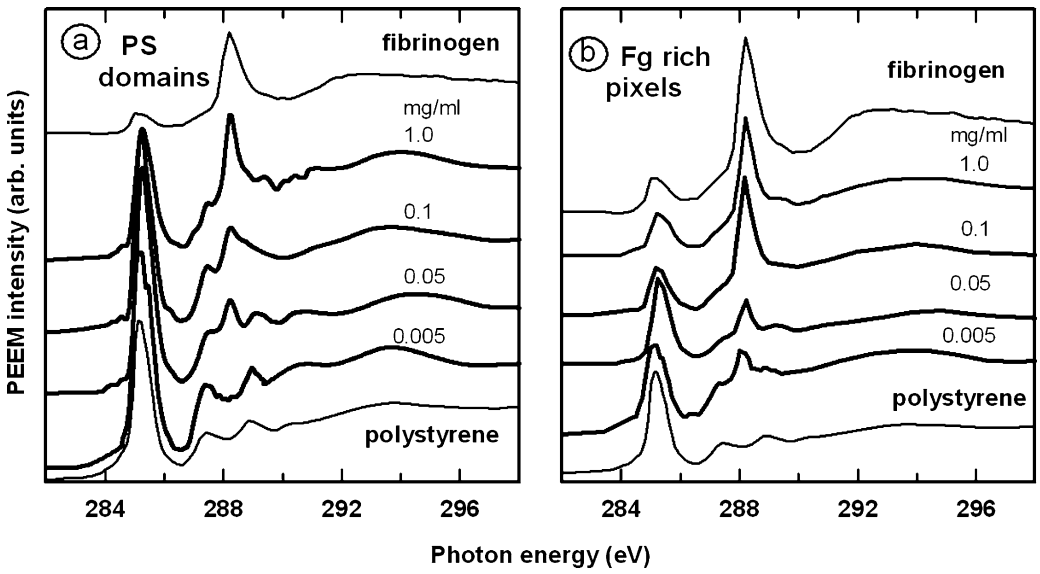


Fig. 5. (a) Spectra from high-PS pixels of the PS component maps generated from stack fit analysis of C 1s image sequences recorded for fibrinogen (0.005, 0.01, 0.05 and 1.0 mg/ml in buffer) adsorbed on the PS:PMMA blend surface. (b) Same for spectra of high-Fg pixels of the Fg component map.

Table 2
Composition[a] of selected PS-rich, PMMA-rich and Fg-rich regions from analysis of C 1s image sequences of a PS/PMMA sample exposed for 10 m to phosphate-buffered Fg solution

| Region masked | Relative amounts (%)[b] | | | |
|---|---|---|---|---|
| | PS | PMMA | Fg | Normalization |
| (A) 0.005 mg/ml | | | | |
| PS | 87 | 11 | 1 | 1.43 |
| PMMA | 28 | 64 | 8 | 1.38 |
| Fg | 54 | 5 | 41 | 1.59 |
| (B) 0.05 mg/ml | | | | |
| PS | 79 | 2 | 19 | 1.89 |
| PMMA | 21 | 70 | 9 | 2.32 |
| Fg | 45 | 1 | 55 | 1.71 |
| (C) 0.1 mg/ml | | | | |
| PS | 58 | 6 | 35 | 1.61 |
| PMMA | 21 | 68 | 10 | 1.39 |
| Fg | 28 | 11 | 61 | 1.75 |
| (D) 1.0 mg/ml | | | | |
| PS | 37 | 28 | 35 | 1.47 |
| PMMA | 25 | 63 | 12 | 1.47 |
| Fg | 25 | 31 | 43 | 1.49 |

[a] The values in the table are percentages derived from the average from selected regions (see Fig. 4, for the case of 0.05 mg/ml Fg exposure) of the PS, PMMA and Fg component maps reported by a three-component stack fit analysis (C 1s, O 1s) or a two-component stack fit analysis (N 1s). If the work function of the various parts of the surface, and different systems is the same, the normalization of the intensity of the image sequences (see text) should result in summation of the coefficients to unity. Deviations of that sum from unity indicate systematic errors such as incorrect intensity normalization as well as statistical errors. The normalization factor (right most column) gives a sense of the size of errors.

[b] Standard deviations of the curve fits to the selected region spectra are between $5 \times 10^{-5}$ and $5 \times 10^{-4}$.

isotonic buffered system (Fig. 4), the color composite map derived from the C 1s image sequence (Fig. 6a), shows that the PS domains are a relatively pure red color, indicating significantly less Fg present. Instead one sees irregular but fairly intense blue on the PMMA side of the PS/PMMA boundaries. This indicates that, in this unbuffered system, Fg is adsorbed preferentially at the PS/PMMA interface. This interpretation is supported by the O 1s and particularly by the N 1s composite map. We note that the O 1s spectrum of the PS region (in this case, identified by threshold masking the inverted PMMA component map) shows significant Fg signal. This indicates that there is some Fg on the main portions of the PS domains in addition to the strong interface component.

While the color coded composite maps give a compelling visualization of the spatial registry of the components, one can legitimately ask: “is this simply artistry?”. To unambiguously demonstrate the origin of these signals, the lower three panels in Fig. 6 are the spectra extracted from the PS-rich, PMMA-rich and Fg-rich pixels which are taken from the color coded regions in the inset images in the spectral plots. These regions were selected by defining a region of interest through a threshold masking procedure applied to the component maps. The interface regions (blue spectra) show a strong Fg signature at each core edge, but with measurable PS and PMMA signals also present, while the spectra of the PMMA (green) and PS (red) domains show negligible Fg signal. The curve fit analysis of these thresholded spectra are summarized in Table 3, along with results from a similar analysis of C 1s, N 1s, and O 1s image sequences for a 0.1 mg/ml Fg/PS:PMMA sample.

Even though fresh areas of the sample were selected for each measurement and the acquisition strategy was designed to stay below 10% modification of the most sensitive PMMA

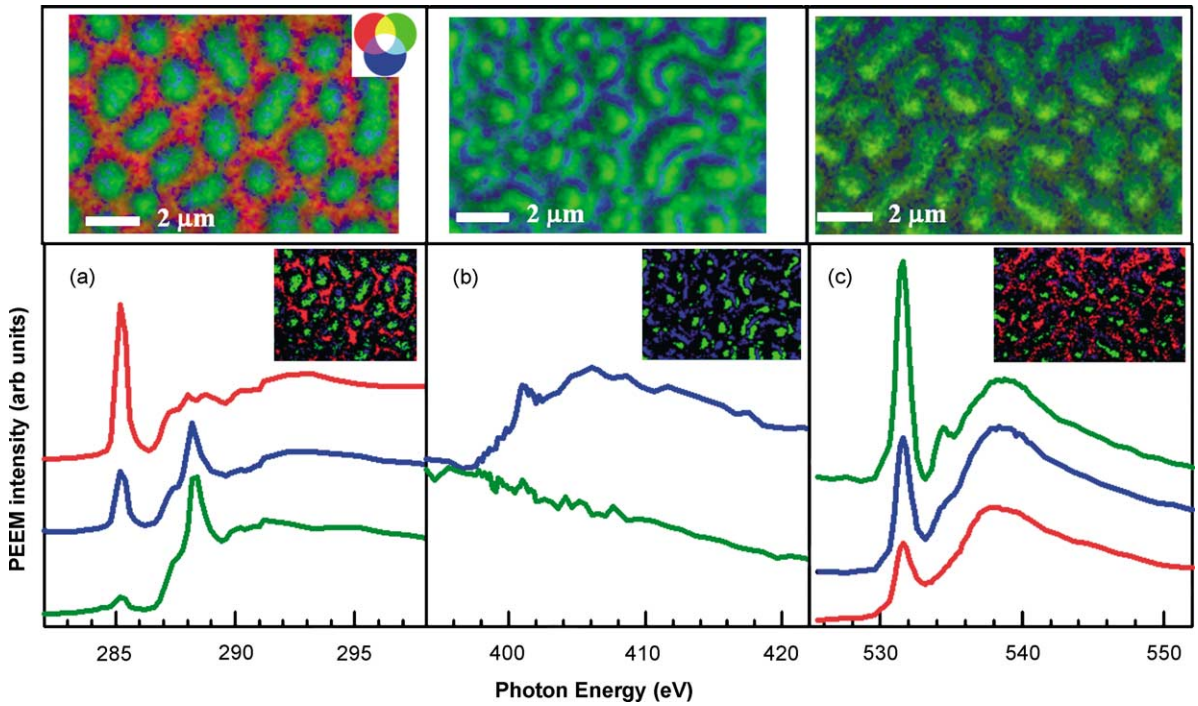


Fig. 6. (a) Color composite map (top) (red: PS; green: PMMA; blue: Fg) and high-PS, high-PMMA and high-Fg spectra derived from a C 1s image sequence recorded for 0.05 mg/ml Fg(water) (bottom). The inset map in the spectral plot indicates the region from which the spectrum was extracted, identified by threshold masking the component maps. (b) Same for N 1s image sequence. In this case, only a two-component fit was carried out (green: PS and PMMA; blue: Fg). (c) Same for O 1s image sequence. The image sequences were collected over three different regions of the sample which is why the domain patterns differ for each core edge study.

component, the radiation dose used was still too high for a damage free analysis. This is indicated by the presence of (excessive) 285 eV signal in the C 1s spectra of PMMA domains and by the intensity of the N 1s $\rightarrow \pi^*$ transition which is lower than in the pure-Fg spectrum (compare Figs. 3 and 6). However, while damage may modify the spectra, the characteristic signatures remain identifiable. The protein is strongly adsorbed (since it could not be washed away) and the sample is dry in the PEEM chamber. Thus, we believe it is very unlikely that the decomposition products would have moved far enough away from the fibrinogen adsorption site to affect the spatial mapping results. In future lower dose conditions will be used to avoid damage artifacts in the spectroscopy.

## 4. Discussion and summary

This work provides the first demonstration that X-PEEM can map selective adsorption of a protein on the different domains of a chemically heterogeneous polymer surface with a spatial resolution better than 0.1 μm. The data from X-PEEM is shown to provide mapping information that is complementary to the total surface concentration data obtained from radiolabeled protein experiments.

Perhaps the most striking result from this study is that at low protein concentration and low ionic strength in unbuffered medium, the protein adsorbs preferentially at the interface between the PS and PMMA domains. This observation is not unexpected from the point of view that proteins are highly surface active and "prefer" the interfacial environment to any other. In this case the interface is among three "phases" (water, PS, PMMA) instead of the more usual two. Presumably attachment at this location is the strongest, and results in the lowest free energy of the system.

The interdomainal location is not preferred when the protein is in isotonic buffer at pH 7.2. Instead, adsorption occurs predominantly on the PS domains. Differences in the behavior of fibrinogen in these two media may be expected on the basis of a difference in net charge due both to different pH (although this difference is small in relation to the isoelectric point of 5.5 for fibrinogen) and/or to charge screening effects at high ionic strength. However, since there are no formal charges on either PMMA or PS, charge effects at low surface coverage should be minimal. Fibrinogen is less soluble in water than in isotonic buffer and thus would be expected to adsorb more extensively from water. However, the similarity of the isotherms at low coverage (Fig. 2) suggests that the effects of any small solubility difference may be negligible: indeed, the $^{125}$I-radiolabeling shows that adsorption is lower from water than from buffer. For the moment there is no obvious reason for the difference in adsorption patterns from the two media. It may be speculated that conformational effects may play a role in these phenomena.

Table 3
Composition[a] of selected PS-rich, PMMA-rich and Fg-rich regions from analysis of C 1s, N 1s, and O 1s image sequences of a Fg(water)/PS:PMMA samples

| Region masked | Relative amounts (%)[b] | | | |
|---|---|---|---|---|
| | PS | PMMA | Fg | Normalization |
| (A) 0.05 mg/ml Fg(water) | | | | |
| C 1s | | | | |
| PS | 77 | 23 | 0 | 1.79 |
| PMMA | 9 | 72 | 19 | 1.72 |
| Fg | 25 | 31 | 44 | 1.92 |
| N 1s[c] | | | | |
| PS/PMMA | – | 91 | 9 | 0.85 |
| Fg | – | 29 | 71 | 1.03 |
| O 1s | | | | |
| PS | 30 | 0 | 70 | 1.02 |
| PMMA | 79 | 17 | 4 | 0.72 |
| Fg | 0 | 19 | 81 | 0.82 |
| (B) 0.1 mg/ml Fg(water) | | | | |
| C 1s | | | | |
| PS | 91 | 0 | 9 | 1.44 |
| PMMA | 14 | 78 | 7 | 1.01 |
| Fg | 67 | 13 | 21 | 1.59 |
| N 1s[c] | | | | |
| PS/PMMA | – | 91 | 9 | 1.03 |
| Fg | – | 36 | 64 | 1.06 |
| O 1s | | | | |
| PS | 32 | 0 | 68 | 0.88 |
| PMMA | 63 | 32 | 5 | 0.68 |
| Fg | 19 | 9 | 72 | 0.93 |

[a] See footnote a of Table 2.
[b] See footnote b of Table 2.
[c] N 1s image sequence was only fit to two components as PS and PMMA are indistinguishable at this edge.

Also, it is possible that the phosphate buffer might play a role in directing Fg to the PS domains. While the beamline used for these measurements did not access the required energies, we intend to measure these types of samples at the P 2p or P 1s core edges in the future in order to rule out co-adsorption with phosphate as the source of the difference in the preferred sites of adsorption. In future studies, the effect of different buffers on adsorption site preference could be investigated.

The present results suggest that, for the 10 min exposure employed, thermodynamic factors (binding affinity) rather than kinetic factors control adsorption. It would be interesting to extend the measurements to shorter exposure times to see if the site preference remains the same or changes in a kinetic-controlled regime.

Using hydrophobicity gradient surfaces, it has been shown convincingly that proteins adsorb more extensively and with greater affinity to hydrophobic compared to hydrophilic surfaces [21,22]. It has also been shown by Rapoza and Horbett [14] that Fg in isotonic buffer adsorbs with greater affinity to hydrophobic compared to hydrophilic surfaces. They found that glassy, rigid polymers (such as PS) showed relatively high fibrinogen adsorption, regardless of whether the polymer was hydrophobic or hydrophilic. However, the binding strength (as measured by elutability) was much lower on hydrophilic polymers and oxygen-containing hydrophobic polymers (such as PMMA). Our results are in accord with these findings in that our radiolabeling data show more extensive adsorption of Fg on PS than on PMMA, and our X-PEEM data show preferential adsorption to the PS domains in the blends at low coverage.

This work has shown that, due to a significant sampling depth, X-PEEM can simultaneously map the chemical structure of a thin film polymer support and sub-monolayer amounts of adsorbed protein. We believe that this approach to the study of protein adsorption will have important applications in the design and surface characterization of biomaterials, e.g. in sub-micron spatial patterning of proteins at the biological–biomaterial interface. These methods may also be useful in other applications where spatial selectivity of adsorption is important (e.g. protein separation and purification). Future work will explore extension of the technique to competitive adsorption in multi-protein systems (e.g. plasma, tear fluid). For these systems, it is anticipated that heavy atom labeling will be required to differentiate proteins one from another.

## Acknowledgements

This research is supported by Natural Science and Engineering Research Council (NSERC, Canada) and the Canada Research Chair programs. X-ray microscopy was carried out using PEEM2 at the ALS (supported by DoE under contract DE-AC03-76SF00098) and the Canadian PEEM at SRC (supported by NSF under award DMR-0084402). The Canadian PEEM was funded by NSERC. Cynthia Morin acknowledges the support of an ALS graduate fellowship during which time most of this work was performed.

## References

[1] D.G. Castner, B.D. Ratner, Surf. Sci. 500 (2002) 28.
[2] M. Tirrell, E. Kokkoli, M. Biesalski, Surf. Sci. 500 (2002) 61.
[3] A.P. Hitchcock, C. Morin, Y.M. Heng, R.M. Cornelius, J.L. Brash, J. Biomater. Sci. Polym. Ed. 13 (2002) 919.
[4] C. Morin, H. Ikeura-Sekiguchi, T. Tyliszczak, R. Cornelius, J.L. Brash, A.P. Hitchcock, A. Scholl, F. Nolting, G. Appel, A.D. Winesett, K. Kaznacheyev, H. Ade, J. Electron. Spectrosc. 121 (2001) 203.
[5] A.L. Bloom, P.T. Thomas (Eds.), Haemostasis and Thrombosis, Churchill Livingstone, New York, 1987.
[6] S.M. Slack, T.A. Horbett, J. Biomater. Sci. Polym. Ed. 2 (1991) 227.
[7] S. Anders, H.A. Padmore, R.M. Duarte, T. Renner, T. Stammler, A. Scholl, M.R. Scheinfein, J. Stöhr, L. Séve, B. Sinkovic, Rev. Sci. Instrum. 70 (1999) 3973.
[8] C. Morin, A.P. Hitchcock, H. Ikeura-Sekiguchi, A. Scholl, A, Doran, K. Kaznacheyev, 2001 ALS Compendium, LBNL Publication, 2002.
[9] C. Morin, A.P. Hitchcock, L. Li, X. Zhang, T. Araki, A. Doran, A. Scholl, manuscript in preparation.

[10] B.L. Henke, E.M. Gullikson, J.C. Davis, At. Data Nucl. Data Tables 54 (1993) 181.
[11] I.N. Koprinarov, A.P. Hitchcock, C. McCrory, R.F. Childs, J. Phys. Chem. B 106 (2002) 5358.
[12] A.P. Hitchcock, et al., Chemical Record, manuscript in preparation.
[13] aXis2000 is a freeware program written in Interactive Data Language (IDL), and available from http://unicorn.mcmaster.ca/aXis2000.html.
[14] R.J. Rapoza, T.A. Horbett, J. Biomed. Mater. Res. 24 (1990) 1263.
[15] Pierce Chemical Company, IODO-GEN Iodination Reagent, 1993.
[16] E. Regoeczi, Iodine-Labeled Plasma Proteins, vol. 1, CRC Press, Boca Raton, FL, 1984.
[17] B.M.C. Chan, J.L. Brash, J. Colloid Interface Sci. 82 (1981) 217.
[18] B.W. Loo Jr., I.M. Sauerwald, A.P. Hitchcock, S.S. Rothman, J. Microsc. 204 (2001) 69.
[19] M. Gordon, G. Cooper, T. Araki, C. Morin, C.C. Turci, K. Kaznatcheev, A.P. Hitchcock, J. Phys. Chem. A 107 (2003) 6144–6159.
[20] J.H. Brown, N. Volkmann, G. Jun, A.H. Henschen-Edman, C. Cohen, Proc. Natl. Acad. Sci. U.S.A. 97 (2000) 85.
[21] H. Elwing, A. Askendal, B. Ivarsson, U. Nilsson, S. Welin, I. Lundstrom, Am. Chem. Soc. Symp. Ser. 343 (1987) 468.
[22] H. Elwing, S. Welin, A. Askendal, U. Nilsson, I. Lundstrom, J. Colloid Interface Sci. 119 (1987) 203.
[23] D.K. Han, G.H. Ryu, K.D. Park, S.Y. Jeong, Y.H. Kim, B.G. Min, J. Biomater. Sci. Polym. Ed. 4 (1993) 401.
[24] R.G. Craig, G.C. Berry, F.A. Peyton, J. Phys. Chem. 64 (1960) 541.